

# Multi-modal Masked Siamese Network Improves Chest X-Ray Representation Learning

**Saeed Shurrab\***

*Department of Computer Engineering  
New York University Abu Dhabi  
Abu Dhabi, United Arab Emirates*

SAEED.SHURRAB@NYU.EDU

**Alejandro Guerra-Manzanares\***

*Department of Computer Engineering  
New York University Abu Dhabi  
Abu Dhabi, United Arab Emirates*

ALEJANDRO.GUERRA@NYU.EDU

**Farah E. Shamout**

*Department of Computer Engineering  
New York University Abu Dhabi  
Abu Dhabi, United Arab Emirates*

FARAH.SHAMOUT@NYU.EDU

*\* These authors contributed equally to this work*

## Abstract

Self-supervised learning methods for medical images primarily rely on the imaging modality during pretraining. While such approaches deliver promising results, they do not leverage associated patient or scan information collected within Electronic Health Records (EHR). Here, we propose to incorporate EHR data during self-supervised pretraining with a Masked Siamese Network (MSN) to enhance the quality of chest X-ray representations. We investigate three types of EHR data, including demographic, scan metadata, and inpatient stay information. We evaluate our approach on three publicly available chest X-ray datasets, MIMIC-CXR, CheXpert, and NIH-14, using two vision transformer (ViT) backbones, specifically ViT-Tiny and ViT-Small. In assessing the quality of the representations via linear evaluation, our proposed method demonstrates significant improvement compared to vanilla MSN and state-of-the-art self-supervised learning baselines. Our work highlights the potential of EHR-enhanced self-supervised pre-training for medical imaging. The code is publicly available at: <https://github.com/nyuad-cai/CXR-EHR-MSN>

## 1. Introduction

Supervised training of deep neural networks requires large amounts of quality annotated data (LeCun et al., 2015). This is not always straightforward in applications involving clinical tasks, due to the time, cost, effort and expertise required to collect labeled data (Taleb et al., 2020). Self-supervised learning has recently demonstrated great success in leveraging unlabeled data, such as in natural language processing (Lan et al., 2019) and computer vision (Jing and Tian, 2020). Such frameworks aim to learn useful underlying representations during pretraining, without any labels, which are then used in downstream prediction tasks via supervised linear evaluation.

Considering the state-of-the-art performance of self-supervised pretraining with large unlabeled data compared to end-to-end supervised learning, a plethora of recent applications in healthcare sought to harness the power of self-supervised learning by focusing on a specific type of data, usually a single modality (Shurrab and Duwairi, 2022). For example, Xie et al. (2020) applied spatial augmentations for 3D image segmentation, while Azizi et al. (2021) applied transformations to Chest X-Ray (CXR) images and dermatology images to predict radiology labels and skin conditions, respectively. Zhang et al. (2022a) preserved time-frequency consistency of time-series data for several tasks, such as detection of epilepsy, while Kiyasseh et al. (2021) leveraged electrocardiogram signals to learn patient-specific representations for classification of cardiac arrhythmia.

In clinical practice, health practitioners rely on several sources of information to perform a diagnosis or interpret medical scans (Cui and Zhang, 2021). For instance, patient sex could be a decisive determinant of diagnostics and therapeutic responses (Mauvais-Jarvis et al., 2020), while patient age could influence clinical decision-making in managing certain health issues (Adams et al., 2006). Health practitioners generally consider additional inputs, such as vital-sign measurements and lab test results, to enhance their understanding of various diseases. Hence, medical data is inherently multi-modal, encompassing various types of modalities, such as medical images, Electronic Health Records (EHR), clinical notes, and omics (Kline et al., 2022). Consequently, we hypothesize that making use of additional modalities during self-supervised pretraining can improve the quality of the representations for downstream classification tasks (Krishnan et al., 2022).

Hence, we propose to incorporate EHR data during self-supervised pretraining with a Masked Siamese Network (Assran et al., 2022) for CXR representation learning. In summary, our pretraining framework includes two visual encoders, adopted from the vanilla MSN, one non-imaging encoder for the EHR, and a projection module that fuses the modalities to encode each CXR-EHR pair. We investigate the inclusion of three types of EHR data, including (a) demographic variables, (b) scan metadata, and (c) inpatient stay information. Our main contributions can be summarized as follows:

- We design a multi-modal MSN to incorporate EHR data during self-supervised pretraining for CXR, with the goal of improving the quality of learned representations and enhancing downstream classification. This specifically involves the introduction of an EHR encoder and projection head for the multimodal representation of EHR and CXR. We compare our approach with vanilla MSN, and compare MSN to other state-of-the-art methods for CXR.
- We conduct a comprehensive evaluation of relevant EHR features, analyzing their individual and combined impact on self-supervised pretraining for downstream classification.
- We extensively evaluate our proposed approach using three publicly available datasets: MIMIC-CXR (Johnson et al., 2019) for pretraining and internal validation, and ChexPert (Irvin et al., 2019) and NIH-14 (Wang et al., 2017) for external validation.

We summarize the related literature in Section 2, our proposed methodology in Section 3, the experimental settings in Section 4, the results in Section 5, and finally the discussion and concluding remarks in Section 6.

## 2. Related Work

### 2.1. Overview of Self-Supervised Learning

Self-supervised learning methods learn task-agnostic feature representations using hand-crafted pretext tasks or joint embedding architectures (Kinakh et al., 2021; Bardes et al., 2021). Hand-crafted pretext tasks rely on the use of pseudo-labels generated from unlabeled data. Examples of such tasks include rotation prediction (Gidaris et al., 2018), jigsaw puzzle solving (Noroozi and Favaro, 2016), colorization (Zhang et al., 2016), and in-painting (Pathak et al., 2016). Joint embedding methods utilize siamese networks (Bromley et al., 1993) to learn useful representations by discriminating between different views of samples based on a specific objective function (Bardes et al., 2021), without the need for human annotation or pseudo-labels.

Joint embedding methods can be further categorized into contrastive and non-contrastive methods, where the latter encompasses clustering, distillation, and information maximization methods (Bardes et al., 2021). Contrastive methods learn representations by maximizing the agreement between positive pairs and minimizing the agreement between negative pairs (Van den Oord et al., 2018). Some prominent examples include SimCLR (Chen et al., 2020), contrastive predictive coding (Van den Oord et al., 2018), and MoCo (He et al., 2020). Non-contrastive methods focus on optimizing different forms of similarity metrics across the learned embeddings. Examples include BYOL (Grill et al., 2020), SimSiam (Chen and He, 2021), and VICReg (Bardes et al., 2021). While most existing work considers convolutional networks as backbones for input encoders, recent approaches explore the role of vision transformers (ViT) (Dosovitskiy et al., 2020) for self-supervision, such as DINO (Caron et al., 2021) and MSN (Assran et al., 2022). MSN is a state-of-the-art self-supervised learning architecture that operates on the principle of mask-denoising, without reconstruction, as well as transformation invariance with transformers. MSN has limited applications in healthcare-related tasks, and is promising considering its computational scalability.

### 2.2. Self-Supervised Learning in Healthcare

Self-supervised learning methods have shown great promise in learning representations of different types of medical images, such as computed tomography and magnetic resonance imaging (Jamaludin et al., 2017; Zhuang et al., 2019; Taleb et al., 2020), optical coherence tomography and fundus photography (Holmberg et al., 2020; Hervella et al., 2020; Li et al., 2021), and endoscopy images (Ross et al., 2018). Several studies investigated self-supervised learning for applications involving CXR images. For example, Sowrirajan et al. (2021), Chen et al. (2021), and Sriram et al. (2021) utilized MoCo (He et al., 2020) as a pretraining strategy for chest disease diagnosis and prognosis tasks. Azizi et al. (2021) showed that initializing SimCLR (Chen et al., 2020) during pretraining with ImageNet weights improves downstream performance in CXR classification. Van der Sluijs et al. (2024) explored the impact of various image augmentation techniques on siamese representation learning for CXR.

Some studies investigated the use of other sources of information in designing the self-supervised learning framework for CXR, mostly focusing on vision-language pretraining. Vu et al. (2021) proposed MedAug, which considers patient metadata for generating pos-

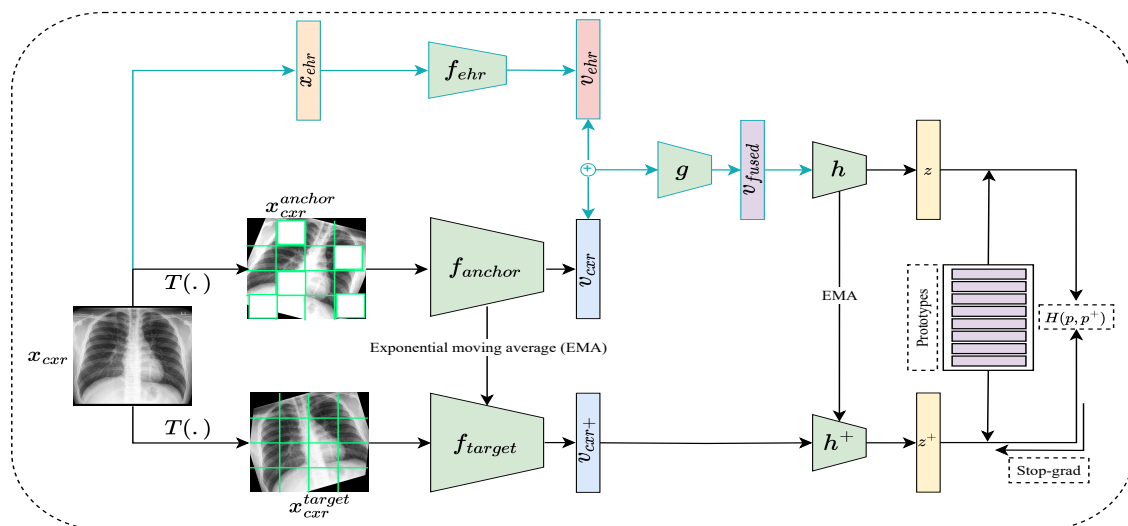


Figure 1: **Overview of the multi-modal MSN pre-training framework.** We use  $x_{ehr}$  as an auxiliary modality during model pretraining. In downstream classification, we freeze  $f_{target}$  and use it as a feature extractor along with a classification head for multi-label image classification. Components of the vanilla MSN are outlined in black.

itive pairs in MoCo framework (He et al., 2020). Tiu et al. (2022) achieved expert-level performance by utilizing raw radiology reports associated with CXR as supervisory signals during self-supervised pretraining. Similarly, Zhang et al. (2022b) proposed ConVIRT, a self-supervised learning framework that learns representations from paired CXR and textual data. None of these methods explored the incorporation of static EHR data during self-supervised pretraining, nor did they investigate the use of MSN for CXR. To address these gaps, we specifically focus on MSN with the goal of enhancing chest X-ray representation learning using transformer pretraining with EHR data.

### 3. Methods

#### 3.1. Problem Formulation

Consider  $x_{cxr} \in \mathbb{R}^{h \times w}$ , where  $h$  and  $w$  represent the image height and width, to be a CXR image collected from patient during their hospital stay, the goal is to predict a set of disease labels  $y_{cxr}$ . We assume that each  $x_{cxr}$  is associated with  $x_{ehr} \in \mathbb{R}^n$ , a vector of static features derived from the patient’s EHR data, where  $n$  is the number of variables. We use both modalities to learn the CXR representation within our pretraining framework. An overview of the multi-modal MSN architecture for pretraining is shown in Figure 1. The network consists of two components: (i) the visual encoders for CXR (ii) a multi-modal branch that incorporates the EHR data, as described in the following sections.

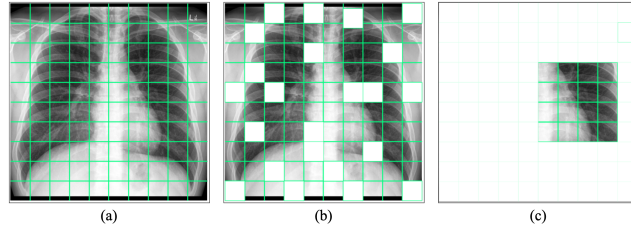


Figure 2: **Visualization of the masking strategies.** (a) Original image. (b) Random masking: drops patches at random locations within the image. (c) Focal masking: keeps a set of neighboring patches and drops the remaining ones.

### 3.2. Masked Siamese Network

We adopt the MSN (Assran et al., 2022) as the base model for our proposed framework due to its computational scalability and the need for pretraining transformers efficiently. For a given unlabeled input image, the goal is to align the anchor and target views, denoted by  $x_{cxr}^{anchor}$  and  $x_{cxr}^{target}$ , respectively. For each image, a random transformation function  $T(\cdot)$  is used to generate a set of  $M$  anchor views and a single target view. The transformations include image resizing, random resized cropping, and random horizontal flipping with a probability of 0.5, following Sowrirajan et al. (2021). However, we excluded color jittering and Gaussian blurring as the former does not apply to grayscale images, while the latter may distort disease-related information (Sowrirajan et al., 2021). Since the views are patchified to serve as input to a ViT, the anchor views are further masked via patch dropping (either random or focal masking as shown in Figure 2), while leaving  $x_{cxr}^{target}$  unmasked.

Two encoders,  $f_{anchor}$  and  $f_{target}$ , parameterized with a ViT (Dosovitskiy et al., 2020), are trained to generate the image embeddings:

$$v_{cxr} = f_{anchor}(x_{cxr}^{anchor}) \ \& \ v_{cxr+} = f_{target}(x_{cxr}^{target}). \quad (1)$$

The target embedding  $v_{cxr+}$  is further processed by a projection head  $h^+$  to obtain  $z^+$ , while  $v_{cxr}$  is used in the multi-modal mapping as described in the next section. MSN does not compute the loss directly on the generated embeddings based on a certain similarity metric. Instead, it utilizes a set of prototypes and seeks to map the projected embeddings of a given sample into the same learned prototype, where the mappings are used to compute the loss. Further background information is provided in Appendix A.

### 3.3. Multi-modal Pretraining

Instead of solely relying on CXR, our proposed framework encourages MSN to leverage additional information extracted from the patient’s EHR. In particular, we introduce three additional modules to the standard MSN architecture. First, we encode the static EHR data with  $f_{ehr}$  to learn a representation vector, such that:

$$v_{ehr} = f_{ehr}(x_{ehr}). \quad (2)$$

We then concatenate ( $\oplus$ ) the EHR and CXR latent representations,  $v_{ehr}$  and  $v_{cxr}$ . At this stage, there exists dimensionality mismatch between the concatenated representations

Table 1: **Summary of EHR features incorporated during pretraining.** We pretrain multi-modal MSN using each of the EHR features summarized below.

Group	Feature	Type	Values	Dimension
Demographic ( $x_D$ )	Age	Numeric	$\{x \in \mathbb{N}   18 \leq x \leq 100\}$	$x_{age} \in \mathbb{R}^1$
	Sex	Binary	$\{Male, Female\}$	$x_{sex} \in \mathbb{R}^2$
Scan medatadata ( $x_{SM}$ )	View	Multiclass	$\{AP, L, PA, LL\}$	$x_{view} \in \mathbb{R}^4$
	Position	Binary	$\{Erect, Recumbent\}$	$x_{pos} \in \mathbb{R}^2$
Inpatient stay information ( $x_{SI}$ )	ICU admission	Binary	$\{Negative, Positive\}$	$x_{icu} \in \mathbb{R}^2$
	In-hospital mortality	Binary	$\{Negative, Positive\}$	$x_{mort} \in \mathbb{R}^2$

Table 2: **Summary of datasets and data splits.** We summarize the size of the training, validation, and test sets in terms of the number of images used in our experiments. We used MIMIC-CXR for self-supervised pretraining and downstream classification and CheXPert to obtain an external test set only. For NIH-14, we used the training set during downstream classification since it has different labels from MIMIC-CXR.

Dataset	Purpose	Training	Validation	Test
<b>MIMIC-CXR</b>	Internal validation	325,188	15,282	36,625
<b>ChexPert</b>	External validation	-	-	688
<b>NIH-14</b>	External validation	32,457	3,567	15,735

and  $v_{cxr+}$ . To address this, we project the concatenated representation into the same dimensional space of  $v_{cxr+}$  using the projection head  $g$ , resulting in  $v_{fused}$ :

$$v_{fused} = g(v_{ehr} \oplus v_{cxr}). \quad (3)$$

Lastly, the fused representation is processed by a projection head  $h(\cdot)$  to compute  $z$ . Both  $z$  and  $z^+$  are used in the clustering of prototypes during pretraining. Overall, this simple procedure learns a joint representation of the EHR data and the anchor embeddings, with the goal of improving the mapping ability of MSN during pretraining.

### 3.4. Downstream Classification

After pretraining the encoders  $f_{target}$ ,  $f_{anchor}$ , and  $f_{ehr}$ , we use  $f_{target}$  as a feature extractor. We then include a classification model  $f_c$  to predict the image labels:

$$\hat{y}_{cxr} = f_c(v_{cxr+}) \quad (4)$$

The main assumption behind our proposed method is that introducing additional data related to the patient or the CXR scan during pretraining would provide the model with valuable contextual information. This information would contribute to enhancing the quality of the learned representations for downstream classification.

## 4. Experiments

### 4.1. Dataset

We conducted our experiments using the MIMIC-CXR dataset, which is a publicly available dataset of CXR images (Johnson et al., 2019). MIMIC-CXR includes 377,110 chest radiographs gathered from 227,835 studies between 2011 and 2016. Each image is associated with a set of ground-truth labels  $y_{cxr} \in \mathbb{R}^{14}$  that indicates the presence of any of 14 medical conditions extracted from corresponding radiology reports. The medical conditions are *Atelectasis*, *Cardiomegaly*, *Consolidation*, *Edema*, *Enlarged Cardiomediastinum*, *Fracture*, *Lung Lesion*, *Lung Opacity*, *Pleural Effusion*, *Pneumonia*, *Pneumothorax*, *Pleural Other*, *Support Devices*, and *No Finding*. After pre-processing, the dataset consisted of 376,201 individual CXR images related to 65,152 patients and 82,506 stays.

We used MIMIC-IV (Johnson et al., 2023), an EHR database associated with MIMIC-CXR, to extract EHR variables related to the CXR images. Table 1 provides a summary of the extracted EHR features, including data types, possible values, and dimensionality. After a thorough investigation of the MIMIC-IV database, we identified three sets of relevant features: patient demographics ( $x_D$ ), scan metadata ( $x_{SM}$ ), and inpatient stay information ( $x_{SI}$ ). For patient demographics, we retrieved patient age ( $x_{age}$ ) for each specific admission and normalized it using *MinMax* normalization, as well as patient sex ( $x_{sex}$ ) encoded as a one-hot vector. For scan metadata, we extracted the scan view ( $x_{view}$ ) and patient position ( $x_{pos}$ ) and encoded them as one-hot vectors. The possible values for view are antero-posterior (AP), lateral (L), postero-anterior (PA), or left-lateral (LL), while for patient position the possible values are erect or recumbent. For inpatient information, we defined  $x_{icu}$  and  $x_{mort}$  as binary features indicating whether the patient required intensive care treatment or experienced in-hospital mortality, respectively. We provide a summary of the EHR features distributions in Appendix B.

We used MIMIC-CXR and MIMIC-EHR for pretraining and downstream classification. We followed the work of Hayat et al. (2022) to obtain the training, validation, and test splits. The data splits are provided in Table 2.

### 4.2. External Validation

We also performed external validation of our pretrained encoders in downstream classification using the ChexPert (Irvin et al., 2019) and National Institutes of Health Chest X-Ray Dataset (NIH-14) (Wang et al., 2017) datasets. ChexPert is a publicly available medical imaging dataset composed of 224,316 chest radiographs of 65,240 patients, collected between 2002-2017, including inpatient and outpatient centers. It includes images and associated radiology reports, which were used to generate labels indicating the presence of 14 diseases. We evaluated the pretrained encoder and classifier obtained with MIMIC-CXR on the ChexPert test set since they have the same labels.

NIH-14 is a publicly available medical imaging dataset composed of 112,120 frontal-view CXR images of 30,805 patients, collected between 1992-2015. Each image is assigned 14 common disease labels. We follow the same split reported in Irvin et al. (2019) and perform linear evaluation using the NIH-14 training set, since it has different labels from MIMIC-CXR. The data splits are shown in Table 2.

### 4.3. Evaluation Protocol

To assess the quality of the learned representations using our proposed pretraining framework, we conducted linear evaluation as the main evaluation protocol following previous work in self-supervised learning (Bardes et al., 2021; Garrido et al., 2023; Huang et al., 2022). We froze the encoder  $f_{target}$  after pretraining, and trained the classification head  $f_c$ , which is randomly initialized, with embeddings of the whole training set.

We report performance using the Area Under the Receiver Operating characteristic Curve (AUROC) and the Area Under the Precision-Recall Curve (AUPRC) across all experiments. We report the 95% Confidence Intervals (CI) using the bootstrapping method (Puth et al., 2015). We also performed statistical significance testing by comparing our proposed approach with the best performing baseline.

### 4.4. Uni-modal Self-supervised Pre-training Baselines

We compared the results of our proposed method with self-supervised and supervised baselines that are transformer-based for a fair comparison:

1. **Vanilla MSN** (Assran et al., 2022): MSN is a self-supervised learning model that leverages the idea of mask-denoising while avoiding pixel and token-level reconstruction. We trained the vanilla version following the architecture in the original work.
2. **DINO** (Caron et al., 2021): DINO is a transformer-based architecture that learns representation via knowledge distillation from a teacher backbone to a student backbone without labels.
3. **Masked AutoEncoder (MAE)** (He et al., 2022): MAE is a transformer-based encoder-decoder architecture that learns representation by reconstructing the missing pixels within an input image.
4. **Supervised**: We train ViT-S and ViT-T in an end-to-end fashion with random and ImageNet (Deng et al., 2009) weight initializations.

In our experiments, we used ViT-Small (ViT-S) as the backbone for our proposed method and the state-of-the-art self-supervised baselines. We also conducted experiments using the ViT-Tiny (ViT-T) backbone. These are smaller versions than the ones defined in Dosovitskiy et al. (2020) and we chose them due to significantly faster training time with comparable performance compared to the original implementation with ViT-Base (ViT-B). All implementation details and model training settings are provided in Appendix A.

## 5. Results

Here, we present the performance results of our proposed method and all self-supervised baselines using the ViT-S. The performance results for ViT-T and all other baselines, including self-supervised and supervised learning methods, are reported in Appendix C.

Table 3: **Performance results for linear evaluation of our proposed method using ViT-S backbone on the MIMIC-CXR dataset.** We summarize the AUROC and AUPRC performance on the test set for the self-supervised methods as well as the 95% confidence intervals. The best results are shown in blue. We use  $\uparrow$  and  $\downarrow$  to indicate whether the performance of a given model is 0.5-1.5% better or worse than the reference model (i.e., vanilla MSN).  $\uparrow\uparrow$  and  $\downarrow\downarrow$  indicate whether the difference is 1.5% better or worse than the reference model, respectively.  $-$  indicates that the performance difference is less than 0.5% compared to the reference model.

Pretraining	AUROC (CI)	AUPRC (CI)
ImageNet	0.703 (0.699, 0.706) $\downarrow\downarrow$	0.269 (0.266, 0.272) $\downarrow\downarrow$
DINO	0.714 (0.711, 0.718) $\downarrow\downarrow$	0.278 (0.276, 0.281) $\downarrow$
MAE	0.649 (0.645, 0.653) $\downarrow\downarrow$	0.223 (0.221, 0.225) $\downarrow\downarrow$
MSN	0.731 (0.727, 0.734)	0.291 (0.289, 0.294)
MSN+ $x_{gen}$	<b>0.751*</b> (0.748, 0.754) $\uparrow\uparrow$	<b>0.311*</b> (0.309, 0.314) $\uparrow\uparrow$
MSN+ $x_{age}$	0.746* (0.743, 0.749) $\uparrow\uparrow$	0.307* (0.305, 0.310) $\uparrow\uparrow$
MSN+ $x_{view}$	0.747* (0.744, 0.750) $\uparrow\uparrow$	0.307* (0.305, 0.310) $\uparrow\uparrow$
MSN+ $x_{pos}$	0.748* (0.745, 0.752) $\uparrow\uparrow$	0.306* (0.303, 0.309) $\uparrow\uparrow$
MSN+ $x_{mort}$	0.748* (0.744, 0.751) $\uparrow\uparrow$	0.308* (0.306, 0.312) $\uparrow\uparrow$
MSN+ $x_{icu}$	0.746* (0.742, 0.749) $\uparrow\uparrow$	0.305* (0.303, 0.308) $\uparrow$
MSN+ $x_{SD}$	<b>0.751*</b> (0.748, 0.754) $\uparrow\uparrow$	0.310* (0.308, 0.313) $\uparrow\uparrow$
MSN+ $x_{SM}$	0.744* (0.741, 0.747) $\uparrow$	0.306* (0.303, 0.309) $\uparrow\uparrow$
MSN+ $x_{IS}$	0.749* (0.746, 0.752) $\uparrow\uparrow$	0.308* (0.305, 0.311) $\uparrow\uparrow$
MSN+ $x_{SD+SM}$	0.742* (0.739, 0.746) $\uparrow$	0.302* (0.300, 0.305) $\uparrow$
MSN+ $x_{SD+SI}$	0.744* (0.740, 0.747) $\uparrow$	0.306* (0.304, 0.309) $\uparrow\uparrow$
MSN+ $x_{SM+SI}$	0.748* (0.744, 0.751) $\uparrow\uparrow$	0.307* (0.304, 0.310) $\uparrow\uparrow$
MSN+ $x_{SD+SM+SI}$	0.739 $\dagger$ (0.736, 0.743) $\uparrow$	0.301* (0.299, 0.305) $\uparrow$

\* Statistical significance results with respect to vanilla MSN ( $p < 0.001$ )

$\dagger$  Statistical significance results with respect to vanilla MSN ( $p < 0.01$ )

### 5.1. Linear Evaluation Results

Table 3 summarizes the performance results of the linear evaluation experiments using ViT-S. First, we note that all of the models that incorporate EHR during pretraining achieve a better performance compared to the best performing baseline, vanilla MSN. The improvement is at least 1% in terms of AUROC and AUPRC, with a maximum improvement of 2% when incorporating demographic information, 0.751 AUROC with  $x_{sex}$  or  $x_D$ , compared to 0.731 AUROC with MSN. Additionally, in most experiments where we pretrain with a single EHR feature achieve improvements greater than 1.5%, while pretraining with groups of features yields slightly lower performance improvements.

Moreover, our proposed strategies demonstrate a significant improvement compared to state-of-the-art self-supervised learning baselines, specifically MAE and DINO, as well as the supervised ImageNet-initialized baseline, reaching an improvement of 10% compared to the worst performing model. In summary, the results of linear evaluation demonstrate that our approach, which incorporates EHR data during pretraining, enhances the quality of the learned representations and downstream performance in a multi-label disease classification task, surpassing both the vanilla MSN and other baselines. In Appendix C, we provide further results with ViT-T as the model backbone. In general, we observe similar patterns, demonstrating consistent behaviour with different backbone architectures.

For the sake of completeness we also report in Appendix C the results of a secondary evaluation protocol by fine-tuning under low data regimes including 1%, 5%, and 10% of

Table 4: **Performance results for external validation of our proposed methods using ViT-S backbone under linear evaluation.** We summarize AUROC and AUPRC results on CheXpert and NIH-14 test sets including 95% confidence intervals. The best results are shown in blue. We use  $\uparrow$  and  $\downarrow$  to indicate whether the performance of a given model is 0.5-1.5% better or worse than the reference model (i.e., vanilla MSN).  $\uparrow\uparrow$  and  $\downarrow\downarrow$  indicate whether the difference is 1.5% better or worse than the reference model, respectively.  $-$  indicates that the performance difference is less than 0.5% compared to the reference model.

Model	CheXpert		NIH-14	
	AUROC (CI)	AUPRC (CI)	AUROC (CI)	AUPRC (CI)
MSN	0.770 (0.755, 0.785)	0.420 (0.409, 0.453)	0.699 (0.695, 0.702)	0.220 (0.217, 0.226)
MSN+ $x_{sex}$	0.768 (0.754, 0.788) $-$	0.417 (0.414, 0.457) $-$	0.734* (0.730, 0.738) $\uparrow\uparrow$	0.265* (0.261, 0.274) $\uparrow\uparrow$
MSN+ $x_{age}$	0.772 (0.754, 0.797) $-$	0.424 (0.416, 0.446) $-$	0.736* (0.732, 0.739) $\uparrow\uparrow$	0.263* (0.257, 0.270) $\uparrow\uparrow$
MSN+ $x_{view}$	<b>0.801<sup>†</sup> (0.785, 0.825)</b> $\uparrow\uparrow$	<b>0.445<sup>†</sup> (0.420, 0.469)</b> $\uparrow\uparrow$	0.732* (0.728, 0.736) $\uparrow\uparrow$	0.261* (0.258, 0.270) $\uparrow\uparrow$
MSN+ $x_{pos}$	0.785 (0.776, 0.798) $\uparrow\uparrow$	0.426 (0.412, 0.465) $\uparrow$	0.734* (0.730, 0.737) $\uparrow\uparrow$	0.261* (0.257, 0.270) $\uparrow\uparrow$
MSN+ $x_{mort}$	0.778 (0.743, 0.811) $\uparrow$	0.424 (0.412, 0.451) $-$	0.737* (0.734, 0.742) $\uparrow\uparrow$	0.265* (0.261, 0.275) $\uparrow\uparrow$
MSN+ $x_{icu}$	0.773 (0.739, 0.789) $-$	0.422 (0.408, 0.445) $-$	0.727* (0.722, 0.731) $\uparrow\uparrow$	0.256* (0.251, 0.264) $\uparrow\uparrow$
MSN+ $x_D$	0.776 (0.757, 0.802) $\uparrow$	0.419 (0.406, 0.439) $-$	0.736* (0.732, 0.740) $\uparrow\uparrow$	0.267* (0.262, 0.276) $\uparrow\uparrow$
MSN+ $x_{SM}$	0.796 <sup>†</sup> (0.775, 0.813) $\uparrow\uparrow$	0.427 (0.418, 0.473) $\uparrow$	0.732* (0.728, 0.735) $\uparrow\uparrow$	0.258* (0.254, 0.268) $\uparrow\uparrow$
MSN+ $x_{SI}$	0.771 (0.753, 0.788) $-$	0.423 (0.402, 0.443) $-$	<b>0.738* (0.734, 0.741)</b> $\uparrow\uparrow$	<b>0.270* (0.264, 0.278)</b> $\uparrow\uparrow$
MSN+ $x_{D+SM}$	0.776 (0.756, 0.791) $\uparrow$	0.412 (0.397, 0.447) $\downarrow$	0.728* (0.725, 0.732) $\uparrow\uparrow$	0.254* (0.250, 0.263) $\uparrow\uparrow$
MSN+ $x_{D+SI}$	0.757 (0.724, 0.769) $\downarrow$	0.418 (0.404, 0.441) $-$	0.728* (0.724, 0.732) $\uparrow\uparrow$	0.269* (0.263, 0.279) $\uparrow\uparrow$
MSN+ $x_{SM+D}$	0.782 (0.761, 0.803) $\uparrow$	0.431 (0.418, 0.452) $\uparrow$	0.734* (0.730, 0.738) $\uparrow\uparrow$	0.263* (0.258, 0.273) $\uparrow\uparrow$
MSN+ $x_{D+SM+SI}$	0.775 (0.753, 0.798) $\uparrow$	0.427 (0.413, 0.452) $\uparrow$	0.725* (0.721, 0.728) $\uparrow\uparrow$	0.251* (0.248, 0.258) $\uparrow\uparrow$

\* Statistical significance results with respect to vanilla MSN ( $p < 0.001$ )

† Statistical significance results with respect to vanilla MSN ( $p < 0.01$ )

the full training set. In this setting, we trained both the pretrained encoder  $f_{target}$  and the classification head  $f_c$  with the training set. We note that the results are on par with vanilla MSN, which is expected since fine-tuning dilutes the effects of incorporating EHR during pretraining.

## 5.2. External Validation Results

Table 4 presents the external validation results for linear evaluation of our proposed methods using the ViT-S backbone on the ChexPert Irvin et al. (2019) and NIH-14 Wang et al. (2017) datasets. The results indicate that our multi-modal pretraining enhances the robustness of self-supervised models, resulting in higher validation scores and improved performance compared to vanilla MSN in most scenarios. In the best scenario, the performance gain reaches 3-4% in both evaluation datasets. However, we observe better performance improvements in the NIH-14 dataset, since its training set was used to train the linear evaluation classifier, compared to off-the-shelf evaluation with CheXpert. The results for the ViT-T backbone and fine-tuning are reported in Appendix C. We observe similar patterns that are in line with the findings of internal validation with MIMIC-CXR.

## 5.3. t-SNE Analysis Results

We applied t-SNE to a subset of samples with a single label in the training set (n=68,000) of MIMIC-CXR for the ease of interpretability, considering the challenge of visualizing multi-label samples in the latent space. Figure 3 visualizes the embeddings obtained with vanilla

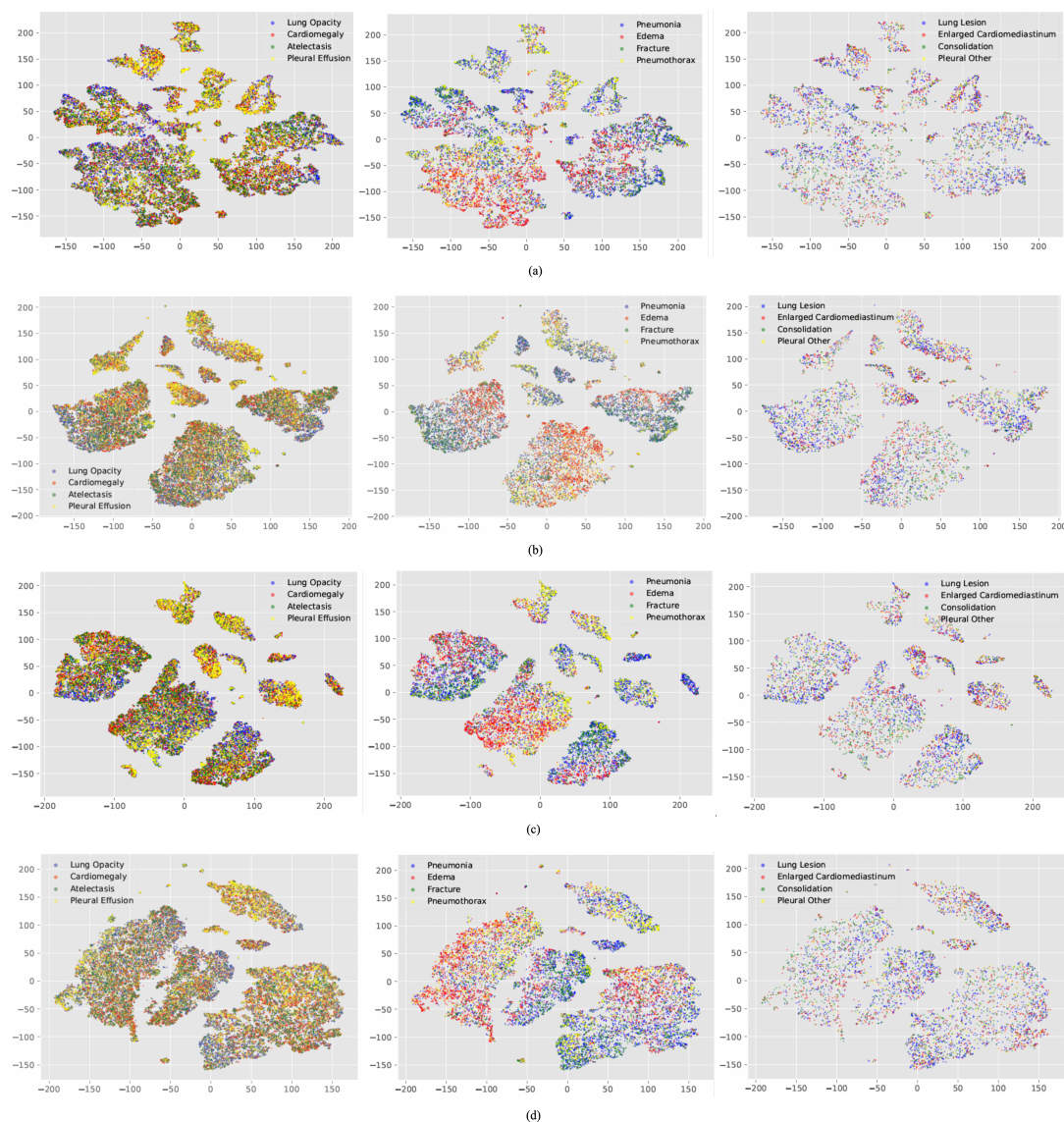


Figure 3: **Embedding visualization via t-SNE.** We plot the resulting embeddings obtained via t-SNE for (a): Vanilla MSN (best performing baseline) (b): MSN+ $x_{sex}$  (best performing proposed variant) (c): MSN+ $x_D$  (best performing proposed variant) (d): MSN+ $x_{D+SM+SI}$  (worst performing proposed variant). The first column depicts the clusters of the four most prevalent diseases in the dataset, the second column corresponds to the second four most prevalent diseases, and the last column represents the four least prevalent diseases.

MSN (baseline), MSN+ $x_{sex}$ , MSN+ $x_D$ , and MSN+ $x_{D+SM+SI}$  for the ViT-S backbone. Based on our qualitative assessment, we observe that the clustering quality is enhanced using MSN+ $x_{sex}$ , MSN+ $x_D$  and MSN+ $x_{D+SM+SI}$  compared to vanilla MSN. More specifically, the clusters of the best performing approaches (MSN+ $x_{sex}$ , and MSN+ $x_D$ ) show

denser clusters, with lower intra-cluster distance and larger inter-cluster distances, which is typically related to a better clustering quality in the embedding space. We hypothesize that this enhanced clustering quality yields an improved downstream performance.

## 6. Discussion

In this paper, we propose the incorporation of EHR data during self-supervised pretraining for CXR representation learning, with the aim of improving performance in downstream classification. We present our proposed approach as an enhanced version of an existing self-supervised learning method, MSN (Assran et al., 2022), by including clinical imaging-related patient EHR data during pretraining. We also comprehensively evaluated our proposed approach on the MIMIC-CXR dataset (internal validation), and two datasets for external validation, ChexPert and NIH-14. Our results demonstrate that the integration of EHR metadata during pretraining with MSN significantly improves performance in the downstream linear evaluation protocol. We also observe that, in general, the inclusion of a single EHR feature yields better quality embeddings compared to pretraining with combinations of EHR features, as shown by the t-SNE embeddings in Figure 3. In addition, our proposed method shows superior performance compared with other state-of-the-art self-supervised baselines, including DINO (Caron et al., 2021) and MAE, (He et al., 2022) as well as fully supervised baselines pretrained with ImageNet (Deng et al., 2009). Our extensive evaluation highlights that our proposed approach generalizes well to external validation datasets, significantly outperforming vanilla MSN in various settings for CheXpert and in all cases for the NIH-14 dataset.

A relevant insight derived from our extensive experimentation using single features and combinations of them is that it is *not guaranteed that the addition of more EHR features leads to improved performance*. We hypothesize that such behavior could be attributed to feature interactions, which is an area of future work.

**Limitations** Despite the performance improvements shown by our framework during linear evaluation, our approach has some limitations. First, our approach did not show significant improvements during end-to-end fine-tuning. That is, it performed on-par with vanilla MSN, or slightly lower in the worst scenario as shown in the additional results in Appendix C. We hypothesize that fine-tuning the target encoder without the EHR data dilutes the impact of incorporating it during pretraining. Specifically, the learned representations during the pretraining stage (with EHR data) are updated during fine-tuning (without EHR data), which impacts the quality of the representations. We aim to address this limitation in our future work, where the EHR data is incorporated during both linear evaluation and fine tuning, rather than solely during pre-training for a fair comparison. Furthermore, we only tested our proposed methodology with a transformer-based self-supervised learning method. In future work, we will explore its applicability to other self-supervised learning architectures and generalization as a framework for other medical imaging datasets and clinical prediction tasks.

## References

- Ann Adams, Christopher D Buckingham, Sara Arber, John B McKinlay, Lisa Marceau, and Carol Link. The influence of patient’s age on clinical decision-making about coronary heart disease in the usa and the uk. *Ageing & society*, 26(2):303–321, 2006.
- Mahmoud Assran, Mathilde Caron, Ishan Misra, Piotr Bojanowski, Florian Bordes, Pascal Vincent, Armand Joulin, Mike Rabbat, and Nicolas Ballas. Masked siamese networks for label-efficient learning. In *European Conference on Computer Vision*, pages 456–473. Springer, 2022.
- Shekoofeh Azizi, Basil Mustafa, Fiona Ryan, Zachary Beaver, Jan Freyberg, Jonathan Deaton, Aaron Loh, Alan Karthikesalingam, Simon Kornblith, Ting Chen, et al. Big self-supervised models advance medical image classification. In *Proceedings of the IEEE/CVF International Conference on Computer Vision*, pages 3478–3488, 2021.
- Adrien Bardes, Jean Ponce, and Yann LeCun. Vicreg: Variance-invariance-covariance regularization for self-supervised learning. *arXiv preprint arXiv:2105.04906*, 2021.
- Jane Bromley, Isabelle Guyon, Yann LeCun, Eduard Säckinger, and Roopak Shah. Signature verification using a” siamese” time delay neural network. *Advances in neural information processing systems*, 6, 1993.
- Mathilde Caron, Hugo Touvron, Ishan Misra, Hervé Jégou, Julien Mairal, Piotr Bojanowski, and Armand Joulin. Emerging properties in self-supervised vision transformers. In *Proceedings of the IEEE/CVF international conference on computer vision*, pages 9650–9660, 2021.
- Ting Chen, Simon Kornblith, Mohammad Norouzi, and Geoffrey Hinton. A simple framework for contrastive learning of visual representations. In *International conference on machine learning*, pages 1597–1607. PMLR, 2020.
- Xiaocong Chen, Lina Yao, Tao Zhou, Jinming Dong, and Yu Zhang. Momentum contrastive learning for few-shot covid-19 diagnosis from chest ct images. *Pattern recognition*, 113: 107826, 2021.
- Xinlei Chen and Kaiming He. Exploring simple siamese representation learning. In *Proceedings of the IEEE/CVF conference on computer vision and pattern recognition*, pages 15750–15758, 2021.
- Miao Cui and David Y Zhang. Artificial intelligence and computational pathology. *Laboratory Investigation*, 101(4):412–422, 2021.
- Jia Deng, Wei Dong, Richard Socher, Li-Jia Li, Kai Li, and Li Fei-Fei. Imagenet: A large-scale hierarchical image database. In *2009 IEEE conference on computer vision and pattern recognition*, pages 248–255. Ieee, 2009.
- Alexey Dosovitskiy, Lucas Beyer, Alexander Kolesnikov, Dirk Weissenborn, Xiaohua Zhai, Thomas Unterthiner, Mostafa Dehghani, Matthias Minderer, Georg Heigold, Sylvain

- Gelly, et al. An image is worth 16x16 words: Transformers for image recognition at scale. *arXiv preprint arXiv:2010.11929*, 2020.
- Quentin Garrido, Randall Balestriero, Laurent Najman, and Yann Lecun. Rankme: Assessing the downstream performance of pretrained self-supervised representations by their rank. In *International Conference on Machine Learning*, pages 10929–10974. PMLR, 2023.
- Spyros Gidaris, Praveer Singh, and Nikos Komodakis. Unsupervised representation learning by predicting image rotations. *arXiv preprint arXiv:1803.07728*, 2018.
- Jean-Bastien Grill, Florian Strub, Florent Alché, Corentin Tallec, Pierre H Richemond, Elena Buchatskaya, Carl Doersch, Bernardo Avila Pires, Zhaohan Daniel Guo, Mohammad Gheshlaghi Azar, et al. Bootstrap your own latent: A new approach to self-supervised learning. *arXiv preprint arXiv:2006.07733*, 2020.
- Nasir Hayat, Krzysztof J Geras, and Farah E Shamout. Medfuse: Multi-modal fusion with clinical time-series data and chest x-ray images. *arXiv preprint arXiv:2207.07027*, 2022.
- Kaiming He, Haoqi Fan, Yuxin Wu, Saining Xie, and Ross Girshick. Momentum contrast for unsupervised visual representation learning. In *Proceedings of the IEEE/CVF conference on computer vision and pattern recognition*, pages 9729–9738, 2020.
- Kaiming He, Xinlei Chen, Saining Xie, Yanghao Li, Piotr Dollár, and Ross Girshick. Masked autoencoders are scalable vision learners. In *Proceedings of the IEEE/CVF Conference on Computer Vision and Pattern Recognition*, pages 16000–16009, 2022.
- Álvaro S Hervella, Lucía Ramos, José Rouco, Jorge Novo, and Marcos Ortega. Multi-modal self-supervised pre-training for joint optic disc and cup segmentation in eye fundus images. In *ICASSP 2020-2020 IEEE International Conference on Acoustics, Speech and Signal Processing (ICASSP)*, pages 961–965. IEEE, 2020.
- Olle G Holmberg, Niklas D Köhler, Thiago Martins, Jakob Siedlecki, Tina Herold, Leonie Keidel, Ben Asani, Johannes Schiefelbein, Siegfried Priglinger, Karsten U Kortuem, et al. Self-supervised retinal thickness prediction enables deep learning from unlabelled data to boost classification of diabetic retinopathy. *Nature Machine Intelligence*, 2(11):719–726, 2020.
- Lang Huang, Chao Zhang, and Hongyang Zhang. Self-adaptive training: Bridging supervised and self-supervised learning. *IEEE transactions on pattern analysis and machine intelligence*, 2022.
- Jeremy Irvin, Pranav Rajpurkar, Michael Ko, Yifan Yu, Silviana Ciurea-Ilcus, Chris Chute, Henrik Marklund, Behzad Haghgoo, Robyn Ball, Katie Shpanskaya, et al. Chexpert: A large chest radiograph dataset with uncertainty labels and expert comparison. In *Proceedings of the AAAI conference on artificial intelligence*, volume 33, pages 590–597, 2019.

- Amir Jamaludin, Timor Kadir, and Andrew Zisserman. Self-supervised learning for spinal mris. In *Deep Learning in Medical Image Analysis and Multimodal Learning for Clinical Decision Support*, pages 294–302. Springer, 2017.
- Longlong Jing and Yingli Tian. Self-supervised visual feature learning with deep neural networks: A survey. *IEEE transactions on pattern analysis and machine intelligence*, 43(11):4037–4058, 2020.
- Alistair EW Johnson, Tom J Pollard, Nathaniel R Greenbaum, Matthew P Lungren, Chih-ying Deng, Yifan Peng, Zhiyong Lu, Roger G Mark, Seth J Berkowitz, and Steven Horng. Mimic-cxr-jpg, a large publicly available database of labeled chest radiographs. *arXiv preprint arXiv:1901.07042*, 2019.
- Alistair EW Johnson, Lucas Bulgarelli, Lu Shen, Alvin Gayles, Ayad Shammout, Steven Horng, Tom J Pollard, Sicheng Hao, Benjamin Moody, Brian Gow, et al. Mimic-iv, a freely accessible electronic health record dataset. *Scientific data*, 10(1):1, 2023.
- Vitaliy Kinakh, Olga Taran, and Svyatoslav Voloshynovskiy. Scatsimclr: self-supervised contrastive learning with pretext task regularization for small-scale datasets. In *Proceedings of the IEEE/CVF International Conference on Computer Vision*, pages 1098–1106, 2021.
- Diederik P Kingma and Jimmy Ba. Adam: A method for stochastic optimization. *arXiv preprint arXiv:1412.6980*, 2014.
- Dani Kiyasseh, Tingting Zhu, and David A Clifton. Clocs: Contrastive learning of cardiac signals across space, time, and patients. In *International Conference on Machine Learning*, pages 5606–5615. PMLR, 2021.
- Adrienne Kline, Hanyin Wang, Yikuan Li, Saya Dennis, Meghan Hutch, Zhenxing Xu, Fei Wang, Feixiong Cheng, and Yuan Luo. Multimodal machine learning in precision health: A scoping review. *npj Digital Medicine*, 5(1):171, 2022.
- Rayan Krishnan, Pranav Rajpurkar, and Eric J Topol. Self-supervised learning in medicine and healthcare. *Nature Biomedical Engineering*, 6(12):1346–1352, 2022.
- Zhenzhong Lan, Mingda Chen, Sebastian Goodman, Kevin Gimpel, Piyush Sharma, and Radu Soricut. Albert: A lite bert for self-supervised learning of language representations. *arXiv preprint arXiv:1909.11942*, 2019.
- Yann LeCun, Yoshua Bengio, and Geoffrey Hinton. Deep learning. *nature*, 521(7553):436–444, 2015.
- Xiaomeng Li, Xiaowei Hu, Xiaojuan Qi, Lequan Yu, Wei Zhao, Pheng-Ann Heng, and Lei Xing. Rotation-oriented collaborative self-supervised learning for retinal disease diagnosis. *IEEE Transactions on Medical Imaging*, 2021.
- Ilya Loshchilov and Frank Hutter. Decoupled weight decay regularization. *arXiv preprint arXiv:1711.05101*, 2017.

- Franck Mauvais-Jarvis, Noel Bairey Merz, Peter J Barnes, Roberta D Brinton, Juan-Jesus Carrero, Dawn L DeMeo, Geert J De Vries, C Neill Epperson, Ramaswamy Govindan, Sabra L Klein, et al. Sex and gender: modifiers of health, disease, and medicine. *The Lancet*, 396(10250):565–582, 2020.
- Paulius Micikevicius, Sharan Narang, Jonah Alben, Gregory Diamos, Erich Elsen, David Garcia, Boris Ginsburg, Michael Houston, Oleksii Kuchaiev, Ganesh Venkatesh, et al. Mixed precision training. *arXiv preprint arXiv:1710.03740*, 2017.
- Mehdi Noroozi and Paolo Favaro. Unsupervised learning of visual representations by solving jigsaw puzzles. In *European conference on computer vision*, pages 69–84. Springer, 2016.
- Deepak Pathak, Philipp Krahenbuhl, Jeff Donahue, Trevor Darrell, and Alexei A Efros. Context encoders: Feature learning by inpainting. In *Proceedings of the IEEE conference on computer vision and pattern recognition*, pages 2536–2544, 2016.
- Marie-Therese Puth, Markus Neuhäuser, and Graeme D Ruxton. On the variety of methods for calculating confidence intervals by bootstrapping. *Journal of Animal Ecology*, 84(4):892–897, 2015.
- Tobias Ross, David Zimmerer, Anant Vemuri, Fabian Isensee, Manuel Wiesenfarth, Sebastian Bodenstedt, Fabian Both, Philip Kessler, Martin Wagner, Beat Müller, et al. Exploiting the potential of unlabeled endoscopic video data with self-supervised learning. *International journal of computer assisted radiology and surgery*, 13(6):925–933, 2018.
- Saeed Shurrab and Rehab Duwairi. Self-supervised learning methods and applications in medical imaging analysis: A survey. *PeerJ Computer Science*, 8:e1045, 2022.
- Hari Sowrirajan, Jingbo Yang, Andrew Y. Ng, and Pranav Rajpurkar. Moco pretraining improves representation and transferability of chest x-ray models. In Matthias Heinrich, Qi Dou, Marleen de Bruijne, Jan Lellmann, Alexander Schläfer, and Floris Ernst, editors, *Proceedings of the Fourth Conference on Medical Imaging with Deep Learning*, volume 143 of *Proceedings of Machine Learning Research*, pages 728–744. PMLR, 07–09 Jul 2021.
- Anuroop Sriram, Matthew Muckley, Koustuv Sinha, Farah Shamout, Joelle Pineau, Krzysztof J Geras, Lea Azour, Yindalon Aphinyanaphongs, Nafissa Yakubova, and William Moore. Covid-19 prognosis via self-supervised representation learning and multi-image prediction. *arXiv preprint arXiv:2101.04909*, 2021.
- Aiham Taleb, Winfried Loetzsch, Noel Danz, Julius Severin, Thomas Gaertner, Benjamin Bergner, and Christoph Lippert. 3d self-supervised methods for medical imaging. *Advances in Neural Information Processing Systems*, 33:18158–18172, 2020.
- Ekin Tiu, Ellie Talius, Pujan Patel, Curtis P Langlotz, Andrew Y Ng, and Pranav Rajpurkar. Expert-level detection of pathologies from unannotated chest x-ray images via self-supervised learning. *Nature Biomedical Engineering*, 6(12):1399–1406, 2022.
- Aaron Van den Oord, Yazhe Li, and Oriol Vinyals. Representation learning with contrastive predictive coding. *arXiv e-prints*, pages arXiv-1807, 2018.

- Rogier Van der Sluijs, Nandita Bhaskhar, Daniel Rubin, Curtis Langlotz, and Akshay S Chaudhari. Exploring image augmentations for siamese representation learning with chest x-rays. In *Medical Imaging with Deep Learning*, pages 444–467. PMLR, 2024.
- Yen Nhi Truong Vu, Richard Wang, Niranjana Balachandar, Can Liu, Andrew Y Ng, and Pranav Rajpurkar. Medaug: Contrastive learning leveraging patient metadata improves representations for chest x-ray interpretation. *arXiv preprint arXiv:2102.10663*, 2021.
- Xiaosong Wang, Yifan Peng, Le Lu, Zhiyong Lu, Mohammadhadi Bagheri, and Ronald M Summers. Chestx-ray8: Hospital-scale chest x-ray database and benchmarks on weakly-supervised classification and localization of common thorax diseases. In *Proceedings of the IEEE conference on computer vision and pattern recognition*, pages 2097–2106, 2017.
- Yutong Xie, Jianpeng Zhang, Zehui Liao, Yong Xia, and Chunhua Shen. Pgl: prior-guided local self-supervised learning for 3d medical image segmentation. *arXiv preprint arXiv:2011.12640*, 2020.
- Richard Zhang, Phillip Isola, and Alexei A Efros. Colorful image colorization. In *European conference on computer vision*, pages 649–666. Springer, 2016.
- Xiang Zhang, Ziyuan Zhao, Theodoros Tsiligkaridis, and Marinka Zitnik. Self-supervised contrastive pre-training for time series via time-frequency consistency. *arXiv preprint arXiv:2206.08496*, 2022a.
- Yuhao Zhang, Hang Jiang, Yasuhide Miura, Christopher D Manning, and Curtis P Langlotz. Contrastive learning of medical visual representations from paired images and text. In *Machine Learning for Healthcare Conference*, pages 2–25. PMLR, 2022b.
- Xinrui Zhuang, Yuexiang Li, Yifan Hu, Kai Ma, Yujiu Yang, and Yefeng Zheng. Self-supervised feature learning for 3d medical images by playing a rubik’s cube. In *International Conference on Medical Image Computing and Computer-Assisted Intervention*, pages 420–428. Springer, 2019.

## Appendix A. Implementation details

In this section, we present additional information pertaining to the implementation details.

### A.1. Masked Siamese Network

The MSN network (Assran et al., 2022) is a self-supervised pretraining architecture that leverages mask de-noising and transformation invariance. Let  $B \geq 1$  be a mini-batch of chest X-ray images sampled from an unlabeled training set. For each image in the dataset, a set of random transformations is applied to obtain  $M$  anchor views  $x_{i,1}, x_{i,2} \dots x_{i,M}$  and a single target view denoted as  $x_i^+$ . As the images serve as input to a Vision Transformer (ViT), the anchor and target views are initially *patchified*, i.e., converted into a set of patches with dimensions  $p \times p$  pixels, where  $p$  represents the patch size. Before the patches are processed by the transformer-based encoders, random and focal masking are applied to the anchor views. Figure 2 illustrates the masking strategies: random masking drops random patches at different locations across the input image, while focal masking drops a block of adjacent patches.

The anchor patches are processed by the encoder  $f_{anchor}$ , while the target patches are processed by the encoder  $f_{target}$  (see Figure 1). The weights of  $f_{target}$  are updated through an exponential moving average of  $f_{anchor}$ . Both encoders are parameterized as ViT encoders. The [CLS] token of each encoder is processed by a three-layer projection head  $h$  to obtain the final image embeddings  $z_{i,m}$  and  $z_i^+ \in \mathbb{R}^n$  for each encoder.

There also exists a set of learnable prototypes  $\mathbf{q} \in \mathbb{R}^{n \times k}$ , where  $K$  is the number of prototypes. The network learns to assign the learned embeddings to the prototypes based on cosine similarity, such that  $p_{i,m} := \text{softmax}(\frac{z_{i,m} \cdot \mathbf{q}}{\tau})$  and  $p_i^+ := \text{softmax}(\frac{z_i^+ \cdot \mathbf{q}}{\tau^+})$ , where  $\tau$  and  $\tau^+$  are the temperature hyperparameters. As described in Assran et al. (2022), the overall loss function is defined using a standard cross-entropy loss  $H(p_i^+, p_{i,m})$  and a mean entropy maximization regularizer  $H(\bar{p})$  following Equation 5:

$$\mathcal{L} = \frac{1}{MB} \sum_{i=1}^B \sum_{m=1}^M H(p_i^+, p_{i,m}) - \lambda H(\bar{p}), \quad (5)$$

where  $B$  is the batch size,  $M$  is the number of anchor views, and  $\lambda$  is the weight of the mean entropy maximization regularizer. The value of  $\bar{p}$  in the regularization term is calculated as presented in Equation 6:

$$\bar{p} = \frac{1}{MB} \sum_{i=1}^B \sum_{m=1}^M p_{i,m} \quad (6)$$

Concerning masking, we use a masking ratio of 0.15 for MSN and 0.6 for MAE. We use exponential moving average with a momentum value of 0.996 to update the *target* encoder in MSN and the *teacher* encoder in DINO, along with their respective projection heads. For focal view generation in MSN, we crop the image to  $96 \times 96$ . We set  $M = 11$  anchor views of an image and generate 1 random mask and 10 focal masks. We also use ImageNet Deng et al. (2009) statistics to normalize the input CXR scans during pretraining.

## A.2. Model Pretraining

We follow the same hyperparameter settings as in the original MSN (Assran et al., 2022), DINO (Caron et al., 2021), and MAE (He et al., 2022). We use the AdamW optimizer (Loshchilov and Hutter, 2017) for MSN and the other self-supervised baselines with a batch size of 64. To select the learning rate, we conduct several experiments using different combinations of learning rate and weight decay values. We empirically found that the best learning rate and weight decay values for MSN are  $1e - 4$  and  $1e - 3$ , respectively, while the best values for DINO and MAE are  $1e - 5$  and  $1e - 4$ , respectively. For all pertaining experiments, we employ the cosine annealing method as a learning rate scheduler. We pretrain each model for 100 epochs with early stopping, using a patience of 5 epochs and a minimum delta of  $1e - 5$  for the training loss.

To incorporate EHR data in our proposal, we implement both  $f_{ehr}$  and  $g$  as linear layers (see Figure 1). We fix the output dimension of  $f_{ehr}$  as 128 and match the output dimension of  $g$  to the hidden size  $D$  according to the backbone used (see Table A1). Table A1 provides an overview of the size and architecture of the Vision Transformer architectures used.

Table A1: **Summary of Vision Transformer (ViT) model variants.** Descriptive summary of the ViT variants employed in our setup and the original Vision Transformer architecture, ViT-Base.

Model	Layers	Hidden size $D$	MLP size	Heads	Parameters
ViT-B	12	768	3072	6	86M
ViT-S	12	384	1536	6	21.7M
ViT-T	12	192	768	6	5.5M

## A.3. Downstream Classification

We use the Adam optimizer (Kingma and Ba, 2014) with a batch size of 64 for all downstream evaluation experiments. For each method evaluation, we perform three experiments with learning rates in  $[1e - 3, 5e - 4, 1e - 4]$  following (Azizi et al., 2021), each with cosine annealing learning rate scheduler. In this setup, we apply early stopping with a patience of 5 epochs if the validation AUROC does not improve by  $1e - 4$ . Additionally, we conduct two more experiments with learning rates in  $[5e - 4, 1e - 4]$  and use the Reduce on Plateau learning rate scheduler without early stopping. We perform this setup once for linear evaluation and replicate it for fine-tuning experiments, resulting in 10 experiments for each model. We select the best-performing model on the validation set for test set evaluation. The maximum training epochs for all downstream evaluation tasks are set to 50 epochs. For augmentations, we apply random horizontal flip, random affine, and center crop during training, and only center crop during inference. We use ImageNet (Deng et al., 2009) statistics to normalize the CXR images during both training and inference, following the same settings as during pretraining.

For low-data regime fine-tuning, we conduct five experiments on five randomly selected subsets of the training set, corresponding to specified percentages (1%, 5%, and 10%), and evaluate the model on the full test set. To run these experiments, we use the same settings

as the best-performing fine-tuning setup on the full training set. The best performing run is selected from the five runs based on the AUROC metric.

All pretraining experiments are conducted using a single Nvidia A100 GPU, and downstream evaluation is performed using a single Nvidia V100 GPU. Pretraining takes approximately 20-30 hours for 100 epochs, while downstream evaluation requires 2-5 hours for 50 epochs, depending on the backbone used. We also enable automatic mixed-precision ([Micikevicius et al., 2017](#)) in all experiments to speed up training and reduce memory requirements.

## Appendix B. EHR Features

Figure B1 provides the frequency distributions for the EHR features considered in our work during the self-supervised pretraining stage.

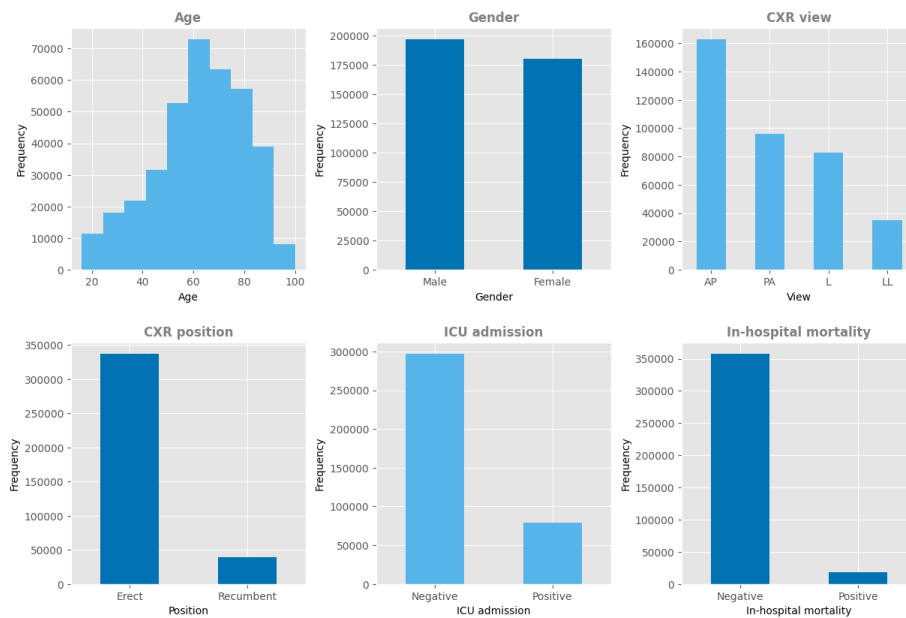


Figure B1: **Distribution of EHR features.** Absolute frequency distributions of the EHR features employed in our experimental setup. Note that the Y-axis in all plots provides the absolute frequency value, but the scale differs.

## Appendix C. Additional Results

In this section, we present additional results from our experimental setting. These results complement or extend the ones provided in the main text, including additional baselines or architectures (i.e., ViT-T).

### C.1. Linear Evaluation

Table C1 provides performance results for linear evaluation of self-supervised methods using the ViT-T architecture as backbone model.

Table C1: **Performance results for linear evaluation of self-supervised methods using ViT-T as backbone model.** We summarize the AUROC and AUPRC performance on the test set for the self-supervised methods as well as the 95% confidence intervals. The best results are shown in blue. We use  $\uparrow$  and  $\downarrow$  to indicate whether the performance of a given model is 0.5-1.5% better or worse than the reference model (i.e., vanilla MSN).  $\uparrow\uparrow$  and  $\downarrow\downarrow$  indicate whether the difference is 1.5% better or worse than the reference model, respectively. – indicates that the performance difference is less than 0.5% compared to the reference model.

Pretraining	AUROC (CI)	AUPRC (CI)
ImageNet	0.684 (0.680, 0.688) $\downarrow\downarrow$	0.251 (0.249, 0.254) $\downarrow\downarrow$
DINO	0.694 (0.691, 0.698) $\downarrow$	0.262 (0.259, 0.264) $\downarrow$
MAE	0.633 (0.629, 0.637) $\downarrow\downarrow$	0.211 (0.209, 0.213) $\downarrow\downarrow$
MSN	0.708 (0.704, 0.711)	0.272 (0.270, 0.275)
MSN+ $x_{sex}$	0.728* (0.724, 0.731) $\uparrow\uparrow$	0.290* (0.288, 0.293) $\uparrow\uparrow$
MSN+ $x_{age}$	0.728* (0.724, 0.732) $\uparrow\uparrow$	0.289* (0.287, 0.292) $\uparrow\uparrow$
MSN+ $x_{view}$	0.726* (0.722, 0.730) $\uparrow\uparrow$	0.288* (0.286, 0.291) $\uparrow\uparrow$
MSN+ $x_{pos}$	<b>0.729*</b> ( <b>0.726, 0.733</b> ) $\uparrow\uparrow$	<b>0.292*</b> ( <b>0.290, 0.295</b> ) $\uparrow\uparrow$
MSN+ $x_{mort}$	0.727* (0.723, 0.730) $\uparrow\uparrow$	0.291* (0.288, 0.294) $\uparrow\uparrow$
MSN+ $x_{icu}$	0.726* (0.722, 0.729) $\uparrow\uparrow$	0.289* (0.287, 0.292) $\uparrow\uparrow$
MSN+ $x_D$	0.727* (0.723, 0.731) $\uparrow\uparrow$	0.290* (0.287, 0.293) $\uparrow\uparrow$
MSN+ $x_{SM}$	0.727* (0.723, 0.730) $\uparrow\uparrow$	0.290* (0.288, 0.293) $\uparrow\uparrow$
MSN+ $x_{SI}$	0.725* (0.721, 0.728) $\uparrow\uparrow$	0.289* (0.286, 0.292) $\uparrow\uparrow$
MSN+ $x_{D+SM}$	0.724* (0.720, 0.727) $\uparrow\uparrow$	0.285* (0.283, 0.288) $\uparrow$
MSN+ $x_{D+SI}$	0.723* (0.720, 0.727) $\uparrow\uparrow$	0.287* (0.285, 0.291) $\uparrow\uparrow$
MSN+ $x_{SM+SI}$	0.726* (0.723, 0.729) $\uparrow\uparrow$	0.288* (0.286, 0.291) $\uparrow\uparrow$
MSN+ $x_{D+SM+SI}$	0.724* (0.720, 0.727) $\uparrow\uparrow$	0.287* (0.284, 0.289) $\uparrow\uparrow$

\* Statistical significance results with respect to vanilla MSN ( $p < 0.001$ )

### C.2. Supervised learning

Table C2 reports performance results of reference architectures trained using supervised learning for comparison with self-supervised methods.

Table C2: **Supervised learning models.** Reference models trained using supervised learning.

Backbone	Initialization	AUROC (CI)	AUPRC (CI)
ViT-T	Random	0.762 (0.758, 0.765)	0.329 (0.326, 0.332)
ViT-T	ImageNet	0.783 (0.780, 0.787)	0.356 (0.353, 0.360)
ViT-S	Random	0.763 (0.759, 0.766)	0.330 (0.328, 0.334)
ViT-S	ImageNet	0.782 (0.778, 0.785)	0.353 (0.350, 0.358)

### C.3. Fine-tuning

Table C3 provides performance results for fine-tuning of self-supervised methods using the ViT-S architecture as backbone model. Table C4 provides the results obtained using ViT-T architecture as backbone.

Table C3: **Performance results for the fine-tuning of our proposed methods using ViT-S as backbone and under low-data regime.** We summarize AUROC and AUPRC results on the test set including 95% confidence intervals. The best results are shown in blue. We use  $\uparrow$  and  $\downarrow$  to indicate whether the performance of a given model is 0.5-1.5% better or worse than the reference model (i.e., vanilla MSN).  $\uparrow\uparrow$  and  $\downarrow\downarrow$  indicate whether the difference is 1.5% better or worse than the reference model, respectively. – indicates that the performance difference is less than 0.5% compared to the reference model.

Pretraining	Training data proportion					
	1%		5%		10%	
	AUROC (CI)	AUPRC (CI)	AUROC (CI)	AUPRC (CI)	AUROC (CI)	AUPRC (CI)
DINO	0.690 (0.687, 0.694) $\downarrow\downarrow$	0.269 (0.267, 0.271) $\downarrow\downarrow$	0.730 (0.727, 0.734) $\downarrow\downarrow$	0.302 (0.300, 0.305) $\downarrow$	0.737 (0.733, 0.740) $\downarrow\downarrow$	0.305 (0.302, 0.308) $\downarrow\downarrow$
MAE	0.659 (0.655, 0.664) $\downarrow\downarrow$	0.241 (0.240, 0.244) $\downarrow\downarrow$	0.702 (0.699, 0.706) $\downarrow\downarrow$	0.274 (0.272, 0.277) $\downarrow\downarrow$	0.727 (0.723, 0.731) $\downarrow\downarrow$	0.297 (0.294, 0.300) $\downarrow\downarrow$
MSN	0.707 (0.703, 0.711)	0.286 (0.284, 0.289)	0.746 (0.743, 0.75)	0.316 (0.313, 0.319)	0.760 (0.756, 0.763)	0.329 (0.327, 0.333)
MSN+ $x_{sex}$	0.713 (0.709, 0.717) $\uparrow$	0.289 (0.287, 0.292) –	0.751 (0.747, 0.754) $\uparrow$	0.315 (0.313, 0.319) –	0.761 (0.758, 0.765) –	0.329 (0.327, 0.333) –
MSN+ $x_{age}$	0.714 (0.710, 0.718) $\uparrow$	0.290 (0.288, 0.293) –	0.751 (0.748, 0.755) $\uparrow$	0.319 (0.316, 0.322) –	0.760 (0.756, 0.763) –	0.326 (0.324, 0.330) –
MSN+ $x_{view}$	0.708 (0.704, 0.711) –	0.282 (0.280, 0.285) –	0.748 (0.744, 0.751) –	0.317 (0.315, 0.320) –	0.761 (0.757, 0.764) –	0.329 (0.327, 0.333) –
MSN+ $x_{pos}$	0.713 (0.710, 0.717) $\uparrow$	0.290 (0.288, 0.292) –	0.749 (0.745, 0.752) –	0.317 (0.315, 0.320) –	0.761 (0.758, 0.764) –	0.329 (0.326, 0.333) –
MSN+ $x_{mort}$	0.711 (0.707, 0.715) –	0.282 (0.279, 0.284) –	0.748 (0.744, 0.751) –	0.317 (0.314, 0.320) –	0.761 (0.757, 0.764) –	0.326 (0.323, 0.329) –
MSN+ $x_{icu}$	0.706 (0.702, 0.710) –	0.284 (0.282, 0.287) –	0.747 (0.744, 0.751) –	0.314 (0.311, 0.317) –	0.758 (0.755, 0.762) –	0.324 (0.321, 0.327) –
MSN+ $x_D$	0.710 (0.706, 0.713) –	0.290 (0.288, 0.293) $\downarrow$	0.749 (0.746, 0.752) –	0.315 (0.313, 0.318) –	0.763 (0.760, 0.766) $\downarrow$	0.330 (0.327, 0.333) $\downarrow$
MSN+ $x_{SM}$	0.710 (0.706, 0.714) –	0.287 (0.285, 0.290) –	0.748 (0.744, 0.751) –	0.315 (0.313, 0.319) –	0.758 (0.755, 0.762) –	0.327 (0.324, 0.330) –
MSN+ $x_{SI}$	0.708 (0.704, 0.712) –	0.286 (0.284, 0.289) –	0.749 (0.746, 0.753) –	0.315 (0.313, 0.318) –	0.762 (0.759, 0.766) –	0.327 (0.325, 0.331) –
MSN+ $x_{D+SM}$	0.704 (0.701, 0.708) –	0.287 (0.285, 0.290) –	0.746 (0.742, 0.749) –	0.314 (0.312, 0.317) –	0.758 (0.754, 0.761) –	0.325 (0.323, 0.329) –
MSN+ $x_{D+SI}$	0.703 (0.699, 0.706) –	0.286 (0.284, 0.288) –	0.745 (0.742, 0.749) –	0.315 (0.313, 0.318) –	0.762 (0.759, 0.765) –	0.328 (0.325, 0.331) –
MSN+ $x_{SM+SI}$	0.708 (0.704, 0.711) –	0.282 (0.280, 0.284) –	0.746 (0.743, 0.750) –	0.315 (0.313, 0.319) –	0.760 (0.757, 0.763) –	0.326 (0.323, 0.329) –
MSN+ $x_{D+SM+SI}$	0.706 (0.702, 0.709) –	0.285 (0.283, 0.288) –	0.746 (0.743, 0.750) –	0.314 (0.312, 0.318) –	0.756 (0.753, 0.759) –	0.326 (0.323, 0.330) –

Table C4: **Performance results for the fine-tuning of our proposed methods using ViT-T as backbone and under low-data regime.** We summarize AUROC and AUPRC results on the test set including 95% confidence intervals. The best results are shown in blue. We use  $\uparrow$  and  $\downarrow$  to indicate whether the performance of a given model is 0.5-1.5% better or worse than the reference model (i.e., vanilla MSN).  $\uparrow\uparrow$  and  $\downarrow\downarrow$  indicate whether the difference is 1.5% better or worse than the reference model, respectively. – indicates that the performance difference is less than 0.5% compared to the reference model.

Pretraining	Training data proportion					
	1%		5%		10%	
	AUROC (CI)	AUPRC (CI)	AUROC (CI)	AUPRC (CI)	AUROC (CI)	AUPRC (CI)
DINO	0.685 (0.682, 0.689) $\downarrow$	0.266 (0.264, 0.268) $\downarrow$	0.727 (0.723, 0.730) $\downarrow\downarrow$	0.297 (0.295, 0.300) $\downarrow$	0.741 (0.737, 0.745) $\downarrow$	0.310 (0.308, 0.313) $\downarrow$
MAE	0.640 (0.636, 0.644) $\downarrow\downarrow$	0.228 (0.227, 0.231) $\downarrow\downarrow$	0.700 (0.697, 0.704) $\downarrow\downarrow$	0.271 (0.269, 0.274) $\downarrow\downarrow$	0.721 (0.717, 0.725) $\downarrow\downarrow$	0.289 (0.286, 0.292) $\downarrow\downarrow$
MSN	0.694 (0.69, 0.698)	0.276 (0.274, 0.279)	0.742 (0.739, 0.746)	0.311 (0.309, 0.314)	0.754 (0.751, 0.758)	0.322 (0.320, 0.326)
MSN+ $x_{sex}$	0.700 (0.696, 0.704) $\uparrow$	0.280 (0.278, 0.283) –	0.739 (0.735, 0.742) –	0.310 (0.308, 0.313) –	0.754 (0.750, 0.758) –	0.320 (0.318, 0.324) –
MSN+ $x_{age}$	0.697 (0.693, 0.701) –	0.278 (0.276, 0.281) –	0.740 (0.737, 0.744) –	0.312 (0.310, 0.315) –	0.753 (0.750, 0.756) –	0.321 (0.318, 0.324) –
MSN+ $x_{view}$	0.698 (0.693, 0.701) –	0.280 (0.278, 0.283) –	0.742 (0.738, 0.746) –	0.310 (0.307, 0.313) –	0.752 (0.748, 0.755) –	0.320 (0.317, 0.323) –
MSN+ $x_{pos}$	0.702 (0.698, 0.705) $\uparrow$	0.279 (0.277, 0.281) –	0.739 (0.734, 0.742) –	0.308 (0.306, 0.312) –	0.754 (0.750, 0.757) –	0.319 (0.316, 0.322) –
MSN+ $x_{mort}$	0.698 (0.694, 0.702) –	0.283 (0.280, 0.285) $\uparrow$	0.738 (0.735, 0.741) –	0.307 (0.305, 0.311) –	0.752 (0.748, 0.755) –	0.318 (0.316, 0.321) –
MSN+ $x_{icu}$	0.700 (0.696, 0.704) $\uparrow$	0.278 (0.276, 0.281) –	0.739 (0.736, 0.743) –	0.308 (0.305, 0.311) –	0.751 (0.748, 0.754) –	0.319 (0.316, 0.322) –
MSN+ $x_D$	0.698 (0.694, 0.701) –	0.273 (0.271, 0.276) –	0.738 (0.734, 0.742) –	0.309 (0.306, 0.311) –	0.752 (0.748, 0.755) –	0.318 (0.316, 0.321) –
MSN+ $x_{SM}$	0.699 (0.695, 0.703) $\uparrow$	0.278 (0.276, 0.281) –	0.740 (0.736, 0.743) –	0.308 (0.306, 0.311) –	0.754 (0.75, 0.757) –	0.322 (0.320, 0.326) $\downarrow$
MSN+ $x_{SI}$	0.702 (0.698, 0.706) $\uparrow$	0.282 (0.280, 0.285) $\uparrow$	0.739 (0.736, 0.743) –	0.309 (0.306, 0.311) –	0.750 (0.746, 0.754) –	0.317 (0.315, 0.320) $\downarrow$
MSN+ $x_{D+SM}$	0.697 (0.693, 0.701) –	0.277 (0.275, 0.280) –	0.735 (0.731, 0.738) $\downarrow$	0.307 (0.304, 0.310) –	0.749 (0.745, 0.752) $\downarrow$	0.317 (0.315, 0.320) $\downarrow$
MSN+ $x_{D+SI}$	0.697 (0.694, 0.701) –	0.278 (0.276, 0.281) –	0.740 (0.737, 0.744) –	0.307 (0.304, 0.310) –	0.753 (0.750, 0.757) –	0.321 (0.318, 0.324) –
MSN+ $x_{SM+SI}$	0.699 (0.694, 0.702) $\uparrow$	0.276 (0.273, 0.278) –	0.739 (0.735, 0.742) –	0.306 (0.304, 0.310) $\downarrow$	0.750 (0.746, 0.753) –	0.316 (0.313, 0.319) $\downarrow$
MSN+ $x_{D+SM+SI}$	0.701 (0.698, 0.705) $\uparrow$	0.280 (0.278, 0.283) –	0.736 (0.733, 0.740) $\downarrow$	0.305 (0.303, 0.308) $\downarrow$	0.752 (0.749, 0.756) –	0.321 (0.319, 0.325) –

#### C.4. External Validation

Table C5 reports external validation results on downstream classification for fine tuning of ViT-S self-supervised models on the ChexPert and NIH-14 datasets.

Table C5: **Performance results for external validation of our proposed methods using ViT-S backbone under fine-tuning self-supervised.** We summarize AUROC and AUPRC results on ChexPert and NIH-14 test sets including 95% confidence intervals. The best results are shown in blue. We use  $\uparrow$  and  $\downarrow$  to indicate whether the performance of a given model is 0.5-1.5% better or worse than the reference model (i.e., vanilla MSN).  $\uparrow\uparrow$  and  $\downarrow\downarrow$  indicate whether the difference is 1.5% better or worse than the reference model, respectively. – indicates that the performance difference is less than 0.5% compared to the reference model.

	CheXpert		NIH-14	
	AUROC (CI)	AUPRC (CI)	AUROC (CI)	AUPRC (CI)
MSN	0.844 (0.827, 0.862)	0.505 (0.483, 0.536)	<b>0.783 (0.780, 0.787)</b>	0.346 (0.339, 0.359)
MSN+ $x_{sex}$	0.850 (0.832, 0.867) $\uparrow$	0.505 (0.480, 0.541) –	0.782 (0.778, 0.787) –	<b>0.350 (0.341, 0.361)</b> –
MSN+ $x_{age}$	0.847 (0.830, 0.863) –	0.491 (0.471, 0.522) $\downarrow$	<b>0.783 (0.779, 0.787)</b> –	<b>0.350 (0.342, 0.360)</b> –
MSN+ $x_{view}$	0.837 (0.819, 0.855) $\downarrow$	0.487 (0.470, 0.514) $\downarrow\downarrow$	0.777 (0.772, 0.781) $\downarrow$	0.338 (0.330, 0.349) $\downarrow$
MSN+ $x_{pos}$	0.836 (0.819, 0.852) $\downarrow$	0.498 (0.476, 0.529) $\downarrow$	0.782 (0.778, 0.785) –	0.343 (0.337, 0.354) –
MSN+ $x_{mort}$	0.841 (0.823, 0.859) –	0.521 (0.494, 0.559) $\uparrow\uparrow$	0.782 (0.776, 0.786) –	0.343 (0.336, 0.356) –
MSN+ $x_{icu}$	0.847 (0.829, 0.867) –	<b>0.510 (0.487, 0.550)</b> $\uparrow$	0.781 (0.778, 0.786) –	0.343 (0.337, 0.354) –
MSN+ $x_D$	0.830 (0.815, 0.846) $\downarrow$	0.477 (0.458, 0.507) $\downarrow\downarrow$	<b>0.783 (0.777, 0.787)</b> –	0.347 (0.339, 0.358) –
MSN+ $x_{SM}$	0.828 (0.807, 0.848) $\downarrow\downarrow$	0.483 (0.464, 0.516) $\downarrow\downarrow$	0.780 (0.776, 0.784) –	0.343 (0.335, 0.353) –
MSN+ $x_{SI}$	0.849 (0.830, 0.866) $\uparrow$	0.492 (0.474, 0.520) $\downarrow$	0.780 (0.776, 0.784) –	0.347 (0.340, 0.357) –
MSN+ $x_{D+SM}$	0.850 (0.830, 0.869) $\uparrow$	<b>0.510 (0.487, 0.546)</b> $\uparrow$	0.775 (0.771, 0.780) $\downarrow$	0.338 (0.331, 0.349) $\downarrow$
MSN+ $x_{D+SI}$	0.827 (0.807, 0.845) $\downarrow\downarrow$	0.480 (0.462, 0.511) $\downarrow\downarrow$	0.776 (0.772, 0.781) $\downarrow$	0.342 (0.335, 0.354) –
MSN+ $x_{SM+D}$	0.834 (0.816, 0.852) $\downarrow$	0.489 (0.470, 0.525) $\downarrow\downarrow$	0.782 (0.778, 0.786) –	0.339 (0.333, 0.347) $\downarrow$
MSN+ $x_{D+SM+SI}$	<b>0.854 (0.835, 0.870)</b> $\uparrow$	0.503 (0.481, 0.534) –	0.775 (0.769, 0.779) $\downarrow$	0.338 (0.331, 0.351) $\downarrow$

Table C6 report external validation results on downstream classification for linear evaluation of ViT-S self-supervised models on the ChexPert and NIH-14 datasets. Table C7 provides the results for the fine-tuning of self-supervised models.

Table C6: **Performance results of external validation for linear evaluation of self-supervised methods using ViT-T as backbone model.** We summarize AUROC and AUPRC results on CheXpert and NIH-14 test sets including 95% confidence intervals. The best results are shown in blue. We use  $\uparrow$  and  $\downarrow$  to indicate whether the performance of a given model is 0.5-1.5% better or worse than the reference model (i.e., vanilla MSN).  $\uparrow\uparrow$  and  $\downarrow\downarrow$  indicate whether the difference is 1.5% better or worse than the reference model, respectively. – indicates that the performance difference is less than 0.5% compared to the reference model.

	CheXpert		NIH-14	
	AUROC (CI)	AUPRC (CI)	AUROC (CI)	AUPRC (CI)
MSN	0.740 (0.720, 0.763)	0.396 (0.382, 0.421)	0.676 (0.671, 0.68)	0.199 (0.197, 0.203)
MSN+ $x_{sex}$	0.742 (0.721, 0.764) –	0.403 (0.389, 0.425) $\uparrow$	0.711* (0.707, 0.714) $\uparrow\uparrow$	0.233* (0.230, 0.242) $\uparrow\uparrow$
MSN+ $x_{age}$	0.767 (0.746, 0.789) $\uparrow\uparrow$	0.390 (0.378, 0.410) $\downarrow$	0.711* (0.707, 0.715) $\uparrow\uparrow$	0.232* (0.229, 0.238) $\uparrow\uparrow$
MSN+ $x_{view}$	0.765 (0.742, 0.788) $\uparrow\uparrow$	<b>0.420*</b> (0.405, 0.453) $\uparrow\uparrow$	0.711* (0.708, 0.715) $\uparrow\uparrow$	0.236* (0.232, 0.245) $\uparrow\uparrow$
MSN+ $x_{pos}$	0.749 (0.728, 0.770) $\uparrow$	0.392 (0.380, 0.411) –	0.710* (0.706, 0.713) $\uparrow\uparrow$	0.235* (0.232, 0.241) $\uparrow\uparrow$
MSN+ $x_{mort}$	0.750 (0.728, 0.772) $\uparrow$	0.413 (0.400, 0.435) $\uparrow\uparrow$	0.709* (0.705, 0.712) $\uparrow\uparrow$	0.236* (0.232, 0.244) $\uparrow\uparrow$
MSN+ $x_{icu}$	0.744 (0.723, 0.765) –	0.398 (0.386, 0.422) –	0.704* (0.700, 0.708) $\uparrow\uparrow$	0.227* (0.225, 0.235) $\uparrow\uparrow$
MSN+ $x_D$	0.746 (0.726, 0.767) $\uparrow$	0.379 (0.368, 0.399) $\downarrow\downarrow$	0.713* (0.709, 0.717) $\uparrow\uparrow$	0.238* (0.235, 0.245) $\uparrow\uparrow$
MSN+ $x_{SM}$	0.766 (0.745, 0.786) $\uparrow\uparrow$	0.402 (0.387, 0.427) $\uparrow$	<b>0.716*</b> (0.712, 0.719) $\uparrow\uparrow$	<b>0.241*</b> (0.236, 0.249) $\uparrow\uparrow$
MSN+ $x_{SI}$	0.765 (0.745, 0.783) $\uparrow\uparrow$	0.387 (0.375, 0.407) $\downarrow$	0.712* (0.708, 0.715) $\uparrow\uparrow$	0.234* (0.231, 0.241) $\uparrow\uparrow$
MSN+ $x_{D+SM}$	0.752 (0.727, 0.778) $\uparrow$	0.391 (0.379, 0.423) $\downarrow$	0.704* (0.700, 0.707) $\uparrow\uparrow$	0.227* (0.224, 0.234) $\uparrow\uparrow$
MSN+ $x_{D+SI}$	0.755 (0.738, 0.777) $\uparrow\uparrow$	0.388 (0.376, 0.408) $\downarrow$	0.709* (0.705, 0.712) $\uparrow\uparrow$	0.233* (0.230, 0.241) $\uparrow\uparrow$
MSN+ $x_{SM+D}$	0.769 (0.752, 0.794) $\uparrow\uparrow$	0.406 (0.403, 0.432) $\uparrow$	0.708* (0.704, 0.711) $\uparrow\uparrow$	0.236* (0.232, 0.243) $\uparrow\uparrow$
MSN+ $x_{D+SM+SI}$	<b>0.770<sup>†</sup></b> (0.746, 0.781) $\uparrow\uparrow$	0.409 (0.403, 0.454) $\uparrow$	0.711* (0.706, 0.716) $\uparrow\uparrow$	0.233* (0.230, 0.240) $\uparrow\uparrow$

\* Statistical significance results with respect to vanilla MSN ( $p < 0.001$ )

† Statistical significance results with respect to vanilla MSN ( $p < 0.01$ )

Table C7: **Performance results of external validation for fine tuning of self-supervised methods using ViT-T as backbone model.** We summarize AUROC and AUPRC results on CheXpert and NIH-14 test sets including 95% confidence intervals. The best results are shown in blue. We use  $\uparrow$  and  $\downarrow$  to indicate whether the performance of a given model is 0.5-1.5% better or worse than the reference model (i.e., vanilla MSN).  $\uparrow\uparrow$  and  $\downarrow\downarrow$  indicate whether the difference is 1.5% better or worse than the reference model, respectively. – indicates that the performance difference is less than 0.5% compared to the reference model.

	CheXpert		NIH-14	
	AUROC (CI)	AUPRC (CI)	AUROC (CI)	AUPRC (CI)
MSN	<b>0.854</b> (0.834, 0.878)	0.494 (0.491, 0.541)	0.773 (0.769, 0.777)	0.330 (0.323, 0.342)
MSN+ $x_{sex}$	0.842 (0.819, 0.854) $\downarrow$	<b>0.510</b> (0.499, 0.540) $\uparrow$	0.768 (0.763, 0.772) $\downarrow$	0.325 (0.318, 0.335) $\downarrow$
MSN+ $x_{age}$	0.846 (0.820, 0.864) $\downarrow$	0.492 (0.467, 0.519) –	0.772 (0.768, 0.776) –	0.330 (0.324, 0.341) –
MSN+ $x_{view}$	0.835 (0.821, 0.849) $\downarrow\downarrow$	0.488 (0.452, 0.514) $\downarrow$	0.776 (0.771, 0.780) –	0.335 (0.328, 0.344) $\uparrow$
MSN+ $x_{pos}$	0.839 (0.819, 0.860) $\downarrow$	0.495 (0.480, 0.533) –	0.768 (0.764, 0.773) $\downarrow$	0.329 (0.322, 0.341) –
MSN+ $x_{mort}$	0.822 (0.806, 0.845) $\downarrow\downarrow$	0.486 (0.484, 0.514) $\downarrow$	0.772 (0.767, 0.776) –	0.326 (0.319, 0.337) –
MSN+ $x_{icu}$	0.832 (0.810, 0.853) $\downarrow\downarrow$	0.465 (0.453, 0.538) $\downarrow\downarrow$	0.769 (0.765, 0.773) –	0.332 (0.325, 0.343) –
MSN+ $x_D$	0.822 (0.811, 0.842) $\downarrow\downarrow$	0.478 (0.466, 0.526) $\downarrow\downarrow$	0.768 (0.763, 0.773) $\downarrow$	0.330 (0.323, 0.341) –
MSN+ $x_{SM}$	0.824 (0.805, 0.831) $\downarrow\downarrow$	0.474 (0.468, 0.501) $\downarrow\downarrow$	0.773 (0.768, 0.777) –	0.335 (0.328, 0.345) –
MSN+ $x_{SI}$	0.829 (0.800, 0.858) $\downarrow\downarrow$	0.491 (0.453, 0.527) –	0.772 (0.768, 0.775) –	0.330 (0.324, 0.340) –
MSN+ $x_{D+SM}$	0.832 (0.804, 0.858) $\downarrow\downarrow$	0.494 (0.475, 0.535) –	0.767 (0.763, 0.771) $\downarrow$	0.318 (0.313, 0.327) $\downarrow$
MSN+ $x_{D+SI}$	0.838 (0.815, 0.848) $\downarrow\downarrow$	0.482 (0.460, 0.515) $\downarrow\downarrow$	<b>0.775</b> (0.770, 0.779) $\uparrow$	<b>0.337</b> (0.330, 0.349) $\uparrow$
MSN+ $x_{SM+D}$	0.840 (0.819, 0.846) $\downarrow$	0.496 (0.484, 0.536) –	0.772 (0.768, 0.777) –	0.334 (0.328, 0.346) –
MSN+ $x_{D+SM+SI}$	0.846 (0.836, 0.866) $\downarrow$	0.492 (0.469, 0.531) –	0.772 (0.767, 0.776) –	0.334 (0.328, 0.344) –